Supplementary Information

Hydrophobic modification of hydroxyl-rich metallic Sn catalysts for acidic CO_2 electroreduction at high current densities

Yuhan Li [a]†, Xinxin Han [a]†, Shanshan Fu[a], Li Guo[a], Shixia Chen[a*], Jun Wang[a*]

[a] School of Chemistry & Chemical Engineering, Nanchang University, Nanchang 330031, People's Republic of China

*Corresponding author.

E-mail for J.W.: jwang7@ncu.edu.cn

E-mail for S.C.: shixiachen@ncu.edu.cn

Characterizations

The morphologies of as-prepared catalysts were conducted by transmission electron microscope (TEM, JEOL JEM-F200) and scanning electron microscope (SEM, ZEISS/Sigma 560). The high-resolution TEM (HRTEM) images and energy-dispersive X-ray spectroscopy (EDS) were also taken by JEOL JEM-F200. The crystal structures of the catalysts were studied by powder X-ray diffraction (XRD) using a Panalytical Empyrean diffractometer with Cu-Kα radiation. The contact angle (CA) characterization of the samples was tested on POWEREACH (IC200D1). The XPS analyses were carried out with a Thermo SCIENTIFIC Nexsa spectrometer using a monochromatic Al Kα source (6 mA, 12 kV). Spectra were calibrated by carbon 1 s spectroscopy with the main line set at 284.8 eV, and then the valence states of the catalysts were analyzed using the Casa XPS software. The detection of hydrogen and carbon monoxide was conducted by gas chromatography (GC 7890). Raman spectroscopy and *in-situ* Raman spectra (LabRAM HR Evolution, France) were collected with a 532 nm laser source. ^{1}H nuclear magnetic resonance (^{1}H NMR) spectra were recorded using an AVANCE 400-MHz NMR instrument.

Preparation of working electrodes

The catalytic activity of CO_2RR in different samples was studied by using a three-electrode flow cell. To prepare the working electrode, the 4 mg catalyst was dispersed in 400 μL ethanol and 40 μL 5% Nafion. The homogeneous catalyst ink with a concentration of 10 mg mL^{-1} was obtained by 1h ultrasound. After 1h ultrasound, the ink was sprayed on a square (1 × 1 cm^2) hydrophobic treated carbon paper (load: 1 mg cm^{-2}) as a cathode electrode for further electrochemical testing. Ag/AgCl electrodes (stored in saturated KCl) and commercial IrTa alloy electrodes were used as reference and counter electrodes, respectively. Nafion 117 was used as the proton exchange membrane to separate the working electrode and the reverse electrode.

Catalysts such as Sn-OH@CMK, Sn-OH@CMK-P, Sn@CMK and SnO_2@CMK can be used directly for electrode preparation after preparation. The concentrations of

PTFE solution required for the samples with optimized PTFE content during the preparation process were 0.025wt%, 0.05wt% and 0.1wt% respectively. The amounts of $SnCl_4 \cdot 5H_2O$ required for the samples with optimized $Sn(OH)_4$ content during the preparation process were 0.1g, 0.2g, 0.4g and 0.8g respectively.

Electrochemical measurements

All electrochemical tests were performed on the CHI660E electrochemical workstation. The catalyst was sprayed on the carbon paper (22BB Gas diffusion layer). The performance of CO_2 reduction was measured by applying different current densities using the time potentiometric method. 0.5 M K_2SO_4 was used as the acid electrolyte (pH = 3). The pH value of the electrolyte was determined by a pH meter. The anode and cathode chambers were both 30 mL, the CO_2 flow rate was 20 sccm, and the electrolyte flow rate was stabilized at 10 mL min^{-1} by the mass flow controller. The duration of each time potentiometric test was 1500 s. Before the test, each catalyst underwent a pre-reduction process at −0.1 A cm^{-2} for 900 s. Before electrolysis, CO_2 gas with a purity of 99.99% was immersed in the electrolyte for 30 min, and the working electrode potential was converted to the RHE reference scale, the formula was as follows:

$$E_{RHE} = E_{Ag/AgCl} + 0.0591 \times pH + 0.197(V)$$

For electrochemical impedance spectroscopy (EIS) measurements, the frequency range was set from 100 000 to 0.1 Hz with an amplitude of 10 mV. The electrochemical double layer capacitance (C_{dl}) of the different samples was determined by the CV method and the electrochemical surface area (ECSA) was then calculated. The linear sweep voltammetry (LSV) plots were measured at a scan rate of 10 mV s^{-1} for the anodic and cathodic reactions. All electrochemical data were not iR-compensation corrected in this work.

In each time potentiometric test, the gas products collected at 1500s are analyzed using gas chromatography (GC, Agilent 7890 gas chromatography system) equipped with a thermal conductivity detector (TCD) and a flame ionization detector (FID).

Argon (99.999%) was used as carrier gas. H_2 was detected by TCD and CO by FID. The liquid products were detected by proton nuclear magnetic resonance (^{1}H NMR, Bruker 400 M) with dimethyl sulfoxide (DMSO) as the internal standard. The Faraday efficiency of H_2, CO, and HCOOH was calculated as follows:

$$FE = e\,F \times n/Q = e\,F \times n / (I \times t) \times 100\%$$

Where e is the number of electrons transferred (for H_2, CO and HCOOH determined as 2), F is the Faraday constant, Q is the charge, I is current, t is the running time and n is the amount of product (in moles) determined by GC or ^{1}H NMR. SPCE for HCOOH was calculated at 25 °C, 1 atm according to the following equation:

$$SPCE_{HCOOH} = (60s \times n) / [\text{flow rate (sccm)} \times t(s)\ 24.05(l/mol)]$$

Where n is the amount of HCOOH (in moles) determined from ^{1}H NMR, and the running time (t) is 1000 s for each flow rate.

Computational details

All the geometries were optimized with Vienna Ab initio Simulation Package (VASP) [1], using the Perdew-Burke-Ernzerhof (PBE) functional[2] and the projector augmented wave (PAW) method [3] to account for core-valence interactions. The kinetic energy cutoff for the plane wave basis set was set to 450 eV. Van der Waals interaction was considered using DFT-D3BJ correction[4,5]. All surface slabs were modeled with a vacuum layer of 15 Å. The convergence threshold was set to 10^{-5} eV energy differences for the electronic SCF step and the convergence threshold for geometry optimization was set to 0.05 eV Å^{-1} for the maximal force. The Gibbs free energy during reactions was defined as follows:

$$\Delta G = E_{ads} - E_{sur} + \Delta H_{corr} - T\Delta S$$

Here, E_{ads} is the electronic energy for the adsorption state; E_{sur} is the electronic energy of the unadsorbed surface; while ΔH_{corr} and ΔS are thermal correction to enthalpy change and entropy change, which were obtained through the aid of VASPKIT, version 1.2.5[6]. the visualization of periodic structures and the analysis of electron density difference are performed by VESTA, Version 3.5.5[7].

107

108

109

110 **Figures**

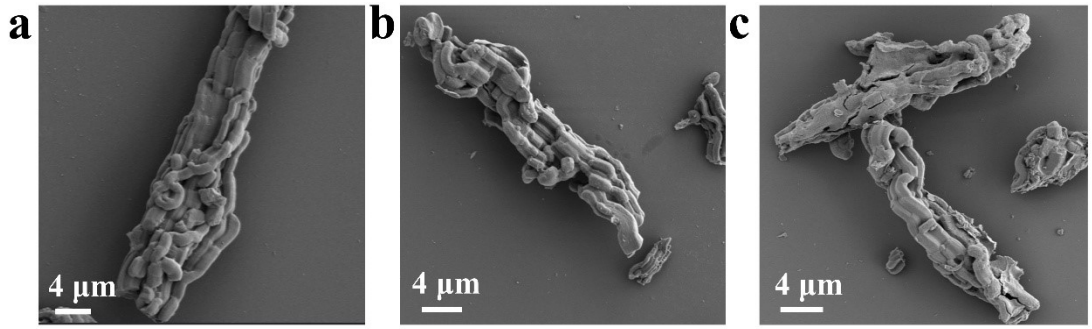

111

112 Fig. S1 SEM image of (a) CMK-3, (b) $Sn(OH)_4$@CMK, (c) $Sn(OH)_4$@CMK-P.

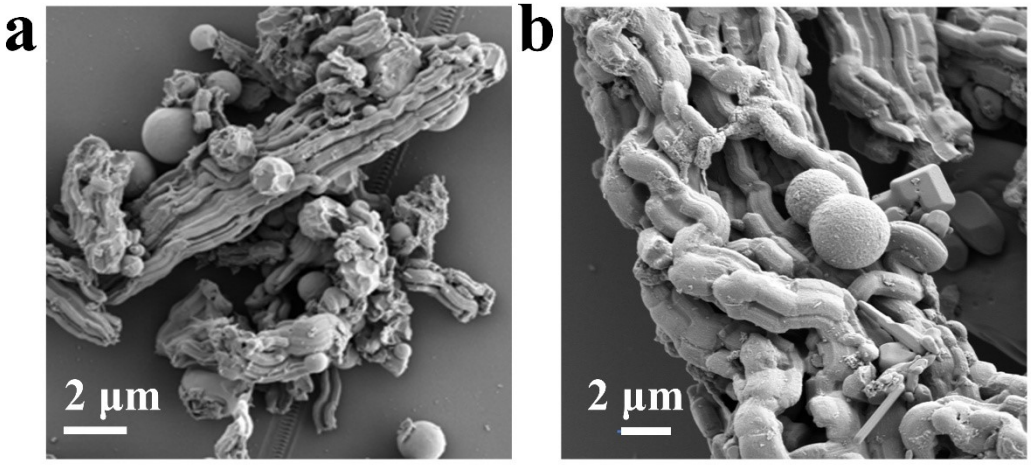

113

114 Fig. S2 SEM image of (a) Sn@CMK, (b) SnO_2@CMK.

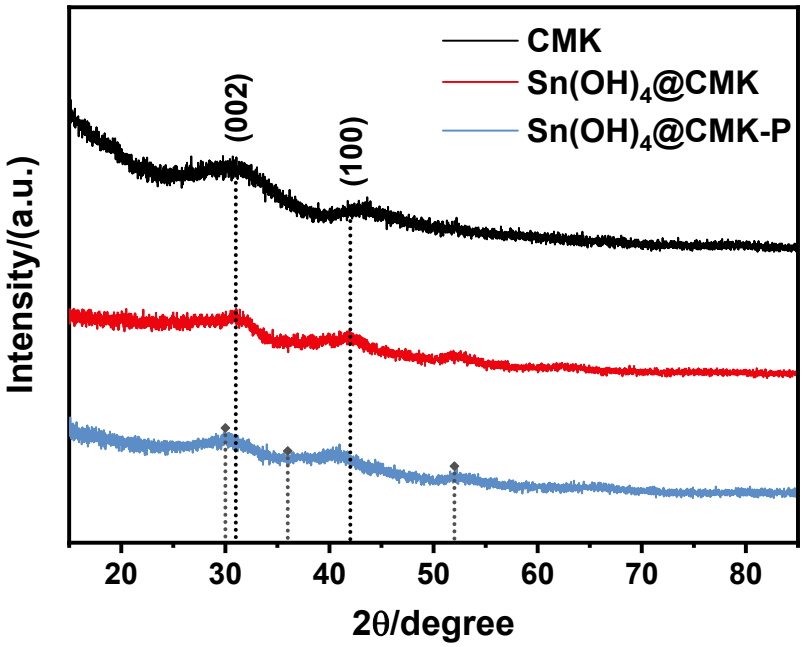

115

116 Fig. S3 XRD patterns of CMK, $Sn(OH)_4$@CMK and $Sn(OH)_4$@CMK-P.

117

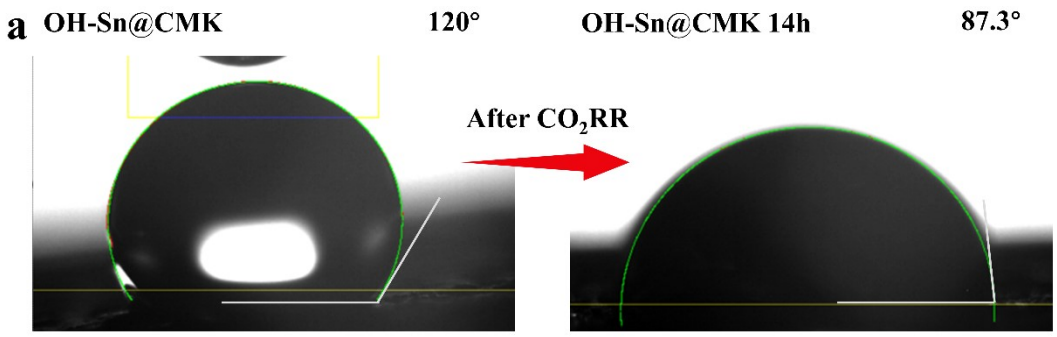

118

119 Fig. S4 Contact angle measured for OH-Sn@CMK.

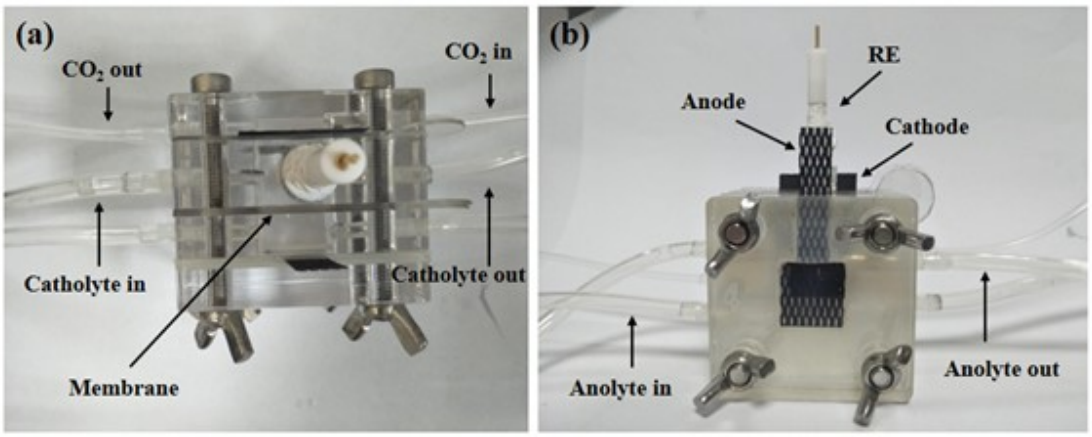

120

121 Fig. S5 Setup image of the used electrochemical flow cell.

122

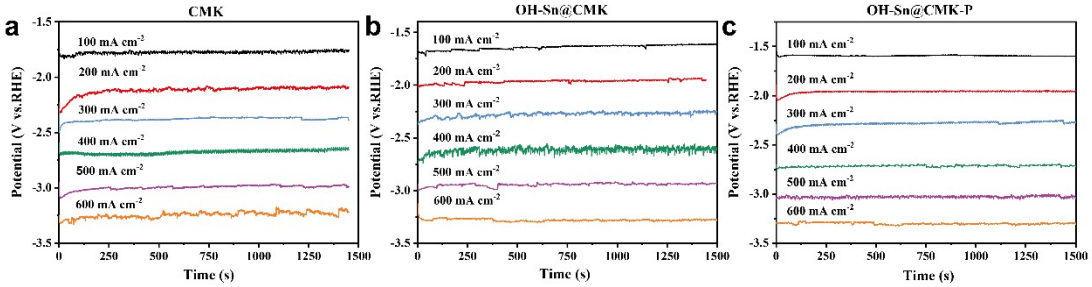

123

124 Fig. S6 Chronopotentiometry (v-t) curves of (a) CMK, (b) OH-Sn@CMK and (c) OH-

125 Sn@CMK-P catalysts.

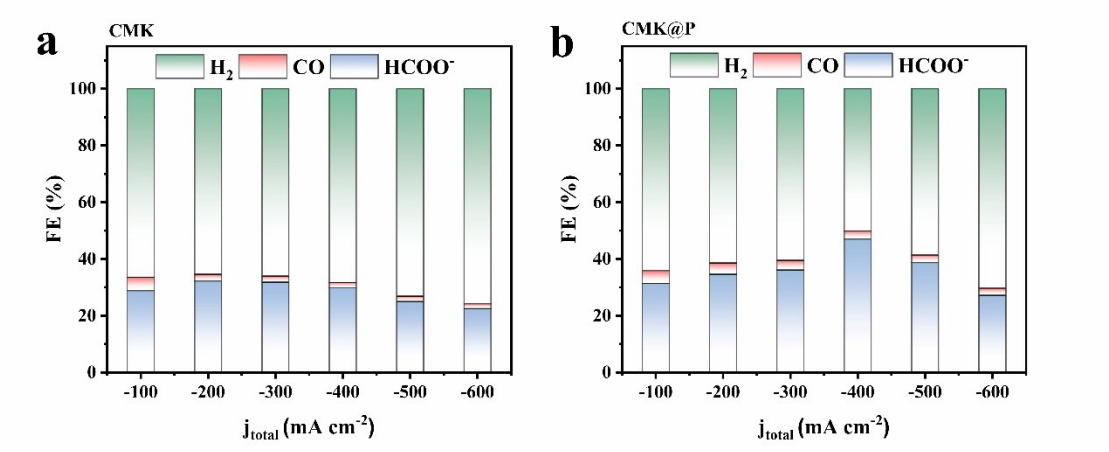

126

127 Fig. S7 The FEs of $HCOO^-$, H_2 and CO for (a) CMK and (b) CMK@P in acidic CO_2RR

128 at pH=3.

129

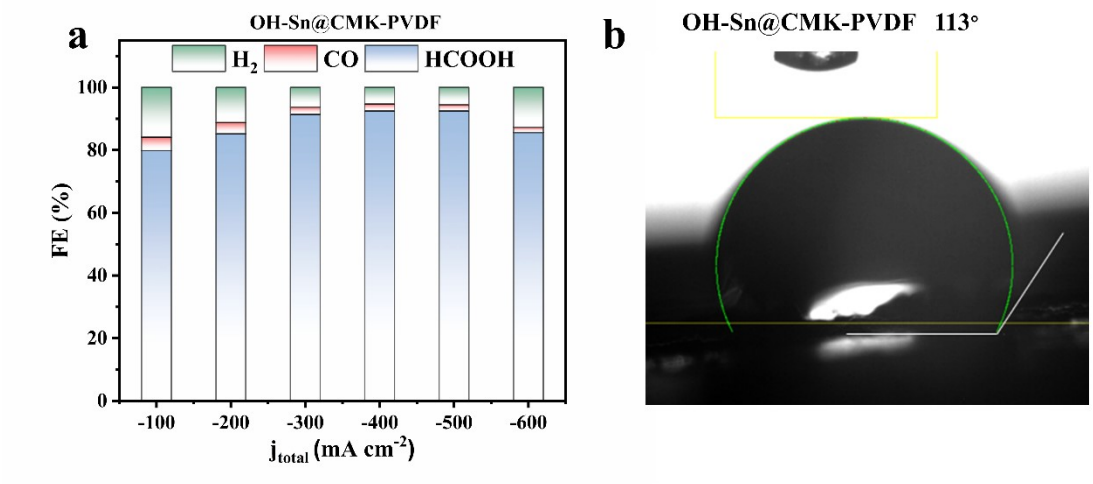

130

131 Fig. S8 (a)The FEs of HCOOH (or $HCOO^-$), H_2, and CO for OH-Sn@CMK-PVDF in

132 acidic CO_2RR. (b) Contact angle measured for OH-Sn@CMK-PVDF after CO_2RR.

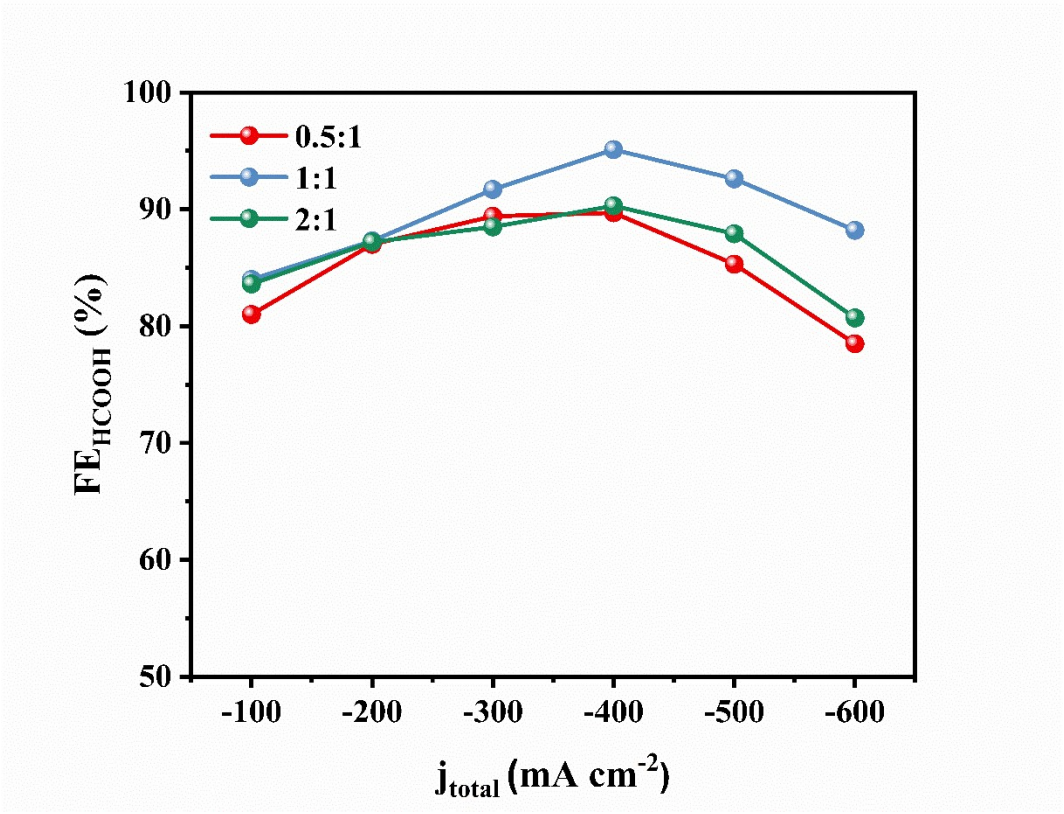

133

134 Fig. S9 The FEs of HCOOH for OH-Sn@CMK-P in acidic CO_2RR at different scale

135 (0.5:1, 1:1, 2:1).

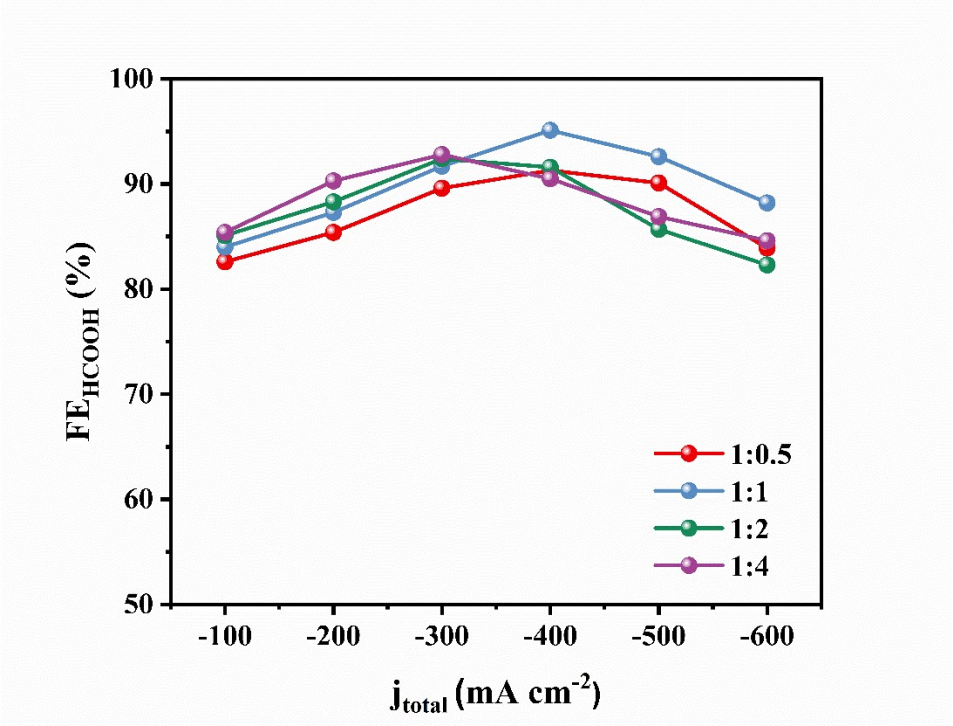

136

137 Fig. S10 FE_{HCOOH} with different $Sn(OH)_4$ content OH-Sn@CMK-P in acidic CO_2RR

138 (CMK: $Sn(OH)_4$ = 1:0.5, 1:1, 1:2, 1:4).

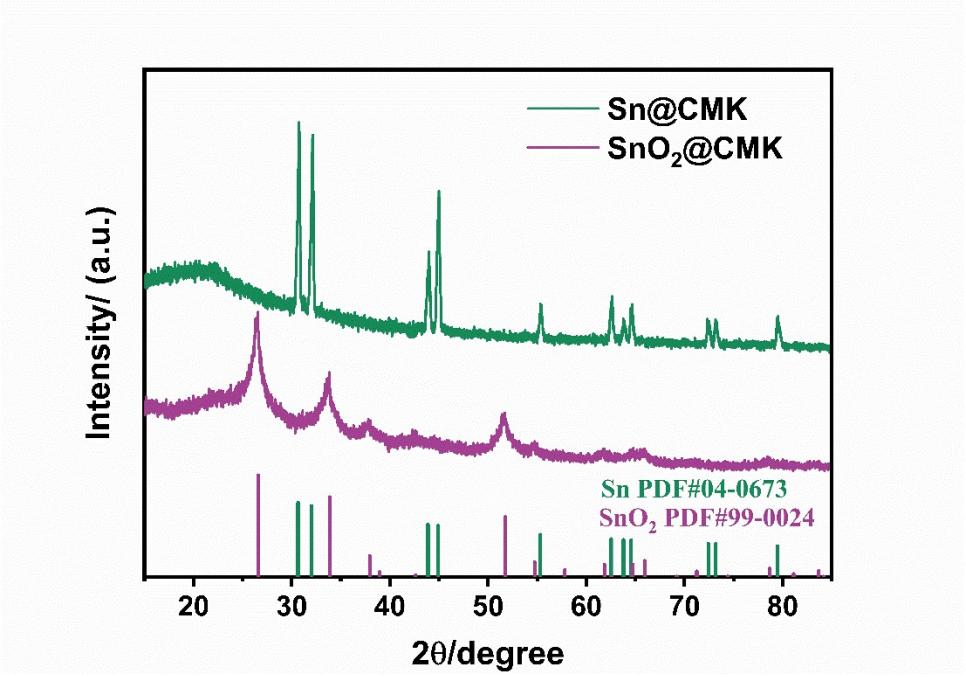

139

140 Fig. S11 XRD patterns of Sn@CMK and SnO_2@CMK.

141

142 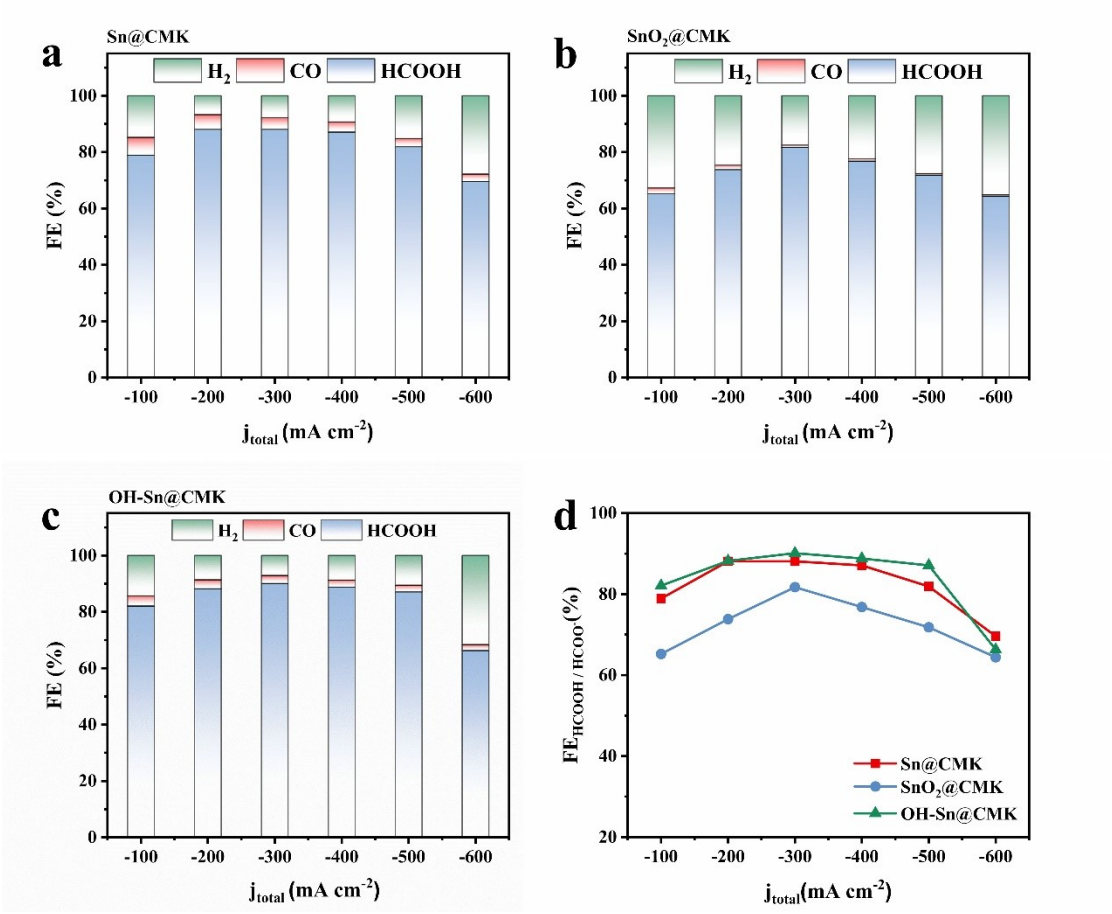

143 Fig. S12 The FEs of HCOOH (or $HCOO^-$), H_2, and CO for (a) Sn@CMK, (b)
144 SnO_2@CMK and (c) OH-Sn@CMK in acidic CO_2RR. (d) Comparison of
145 $FE_{HCOOH/HCOO^-}$ at Sn@CMK, SnO_2@CMK, and OH-Sn@CMK under different
146 currents.

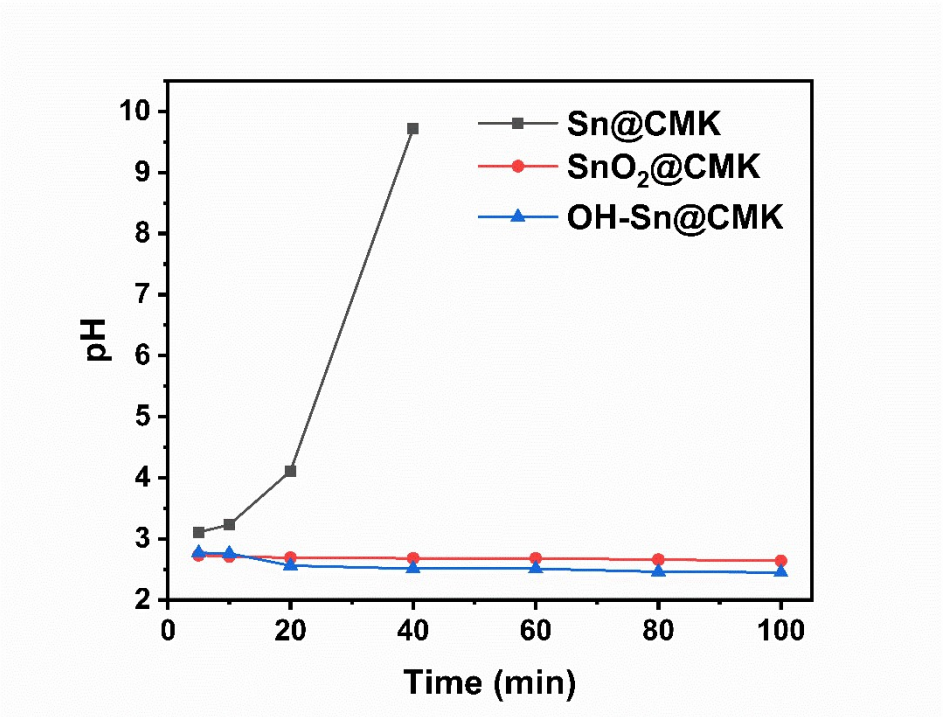

147

148 Fig. S13 Sn@CMK, SnO_2@CMK, and OH-Sn@CMK pH test of electrolytes in
149 electroreduction processes.

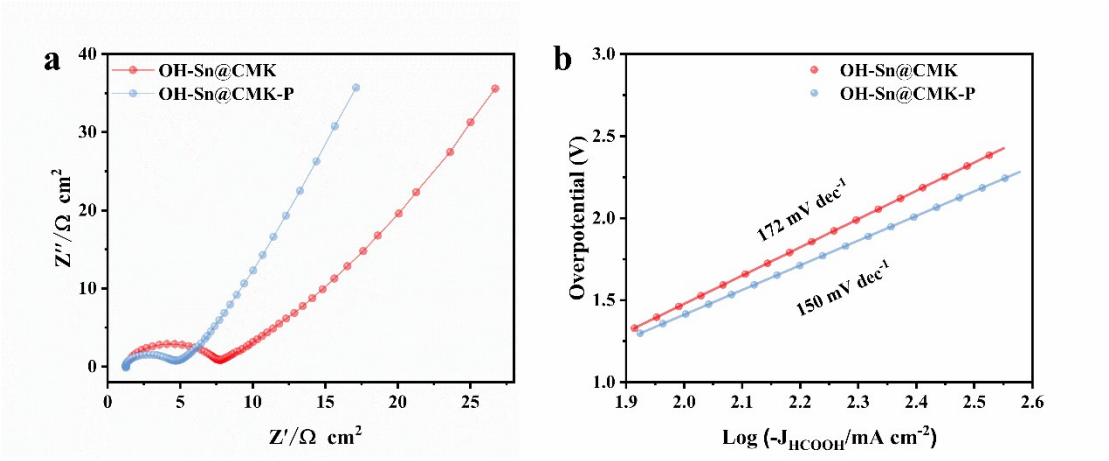

150

151 Fig.S14 (a) EIS and (b) Tafel tests for OH-Sn@CMK and OH-Sn@CMK-P.

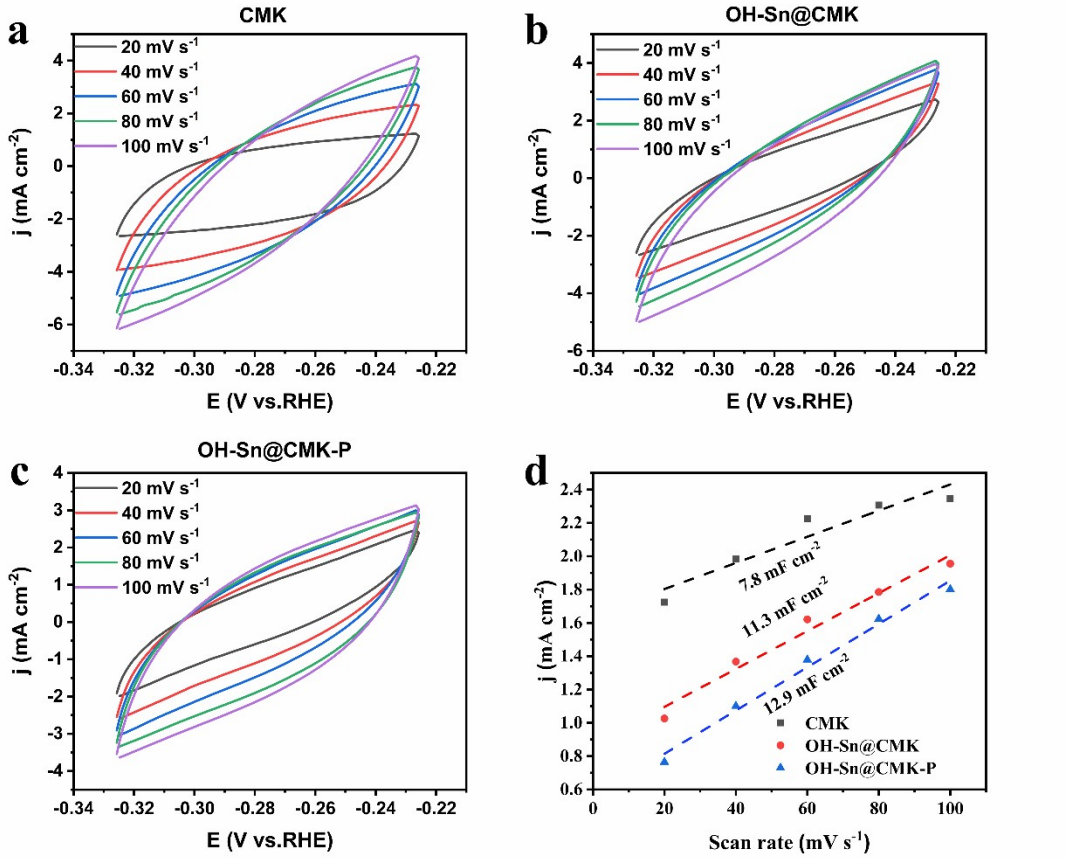

152

153 Fig. S15 Cyclic voltammetry taken over a range of scan rates for (a) CMK, (b) OH-
154 Sn@CMK, and (c) OH-Sn@CMK-P. (d) Current due to double-layer charging plotted
155 against cyclic voltammetry scan rate for CMK, OH-Sn@CMK, and OH-Sn@CMK-P.

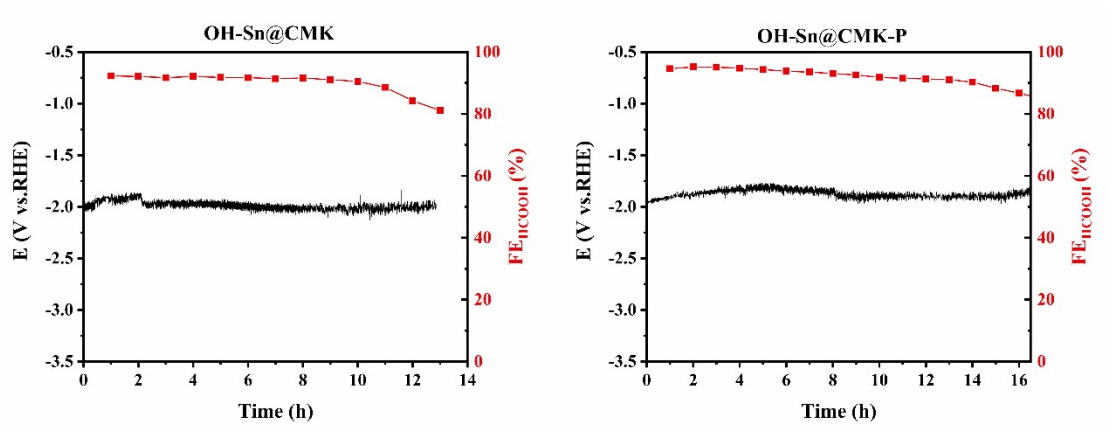

156

157 Fig. S16 The stability of (a) OH-Sn@CMK and (b) OH-Sn@CMK-P at −200 mA cm-
158 ^{2} under the pH=3 electrochemical environment in CO_2RR.

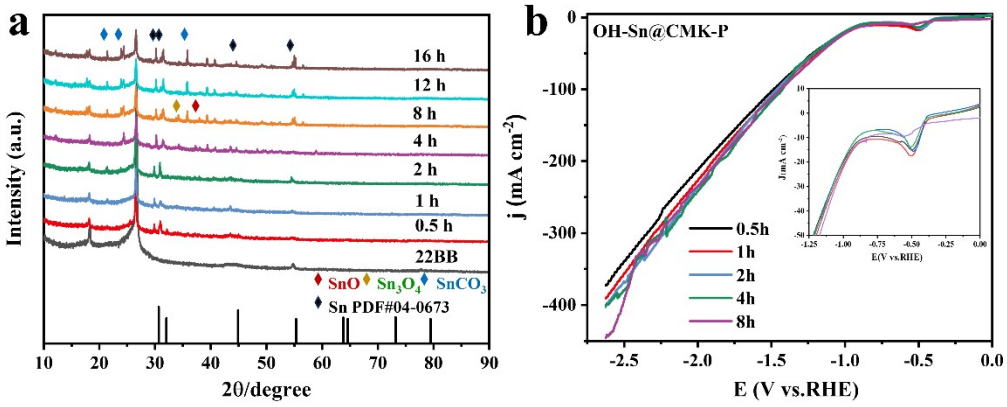

159

160 Fig. S17 (a) XRD and (b) LSV images of OH-Sn@CMK-P catalyst in CO_2RR process.

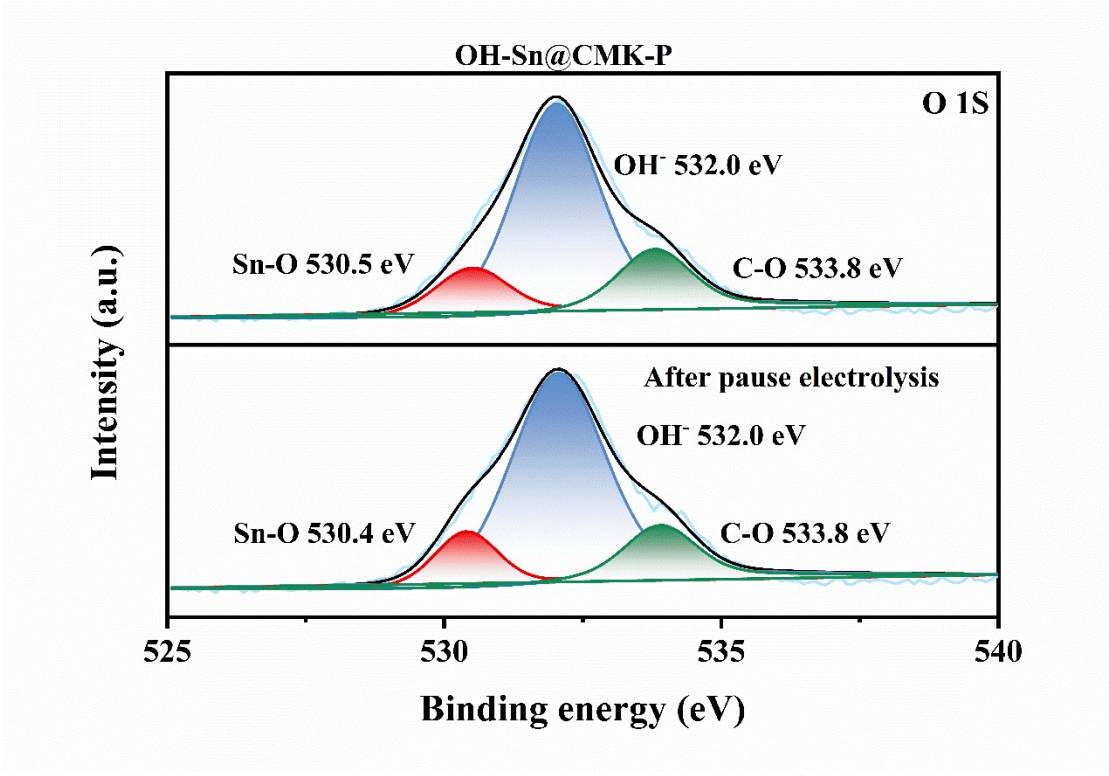

161

162 Fig. S18 The XPS spectrum of the electrode surface of OH-Sn@CMK-P before and

163 after suspension at -200 mA cm^{-2} for 30 min

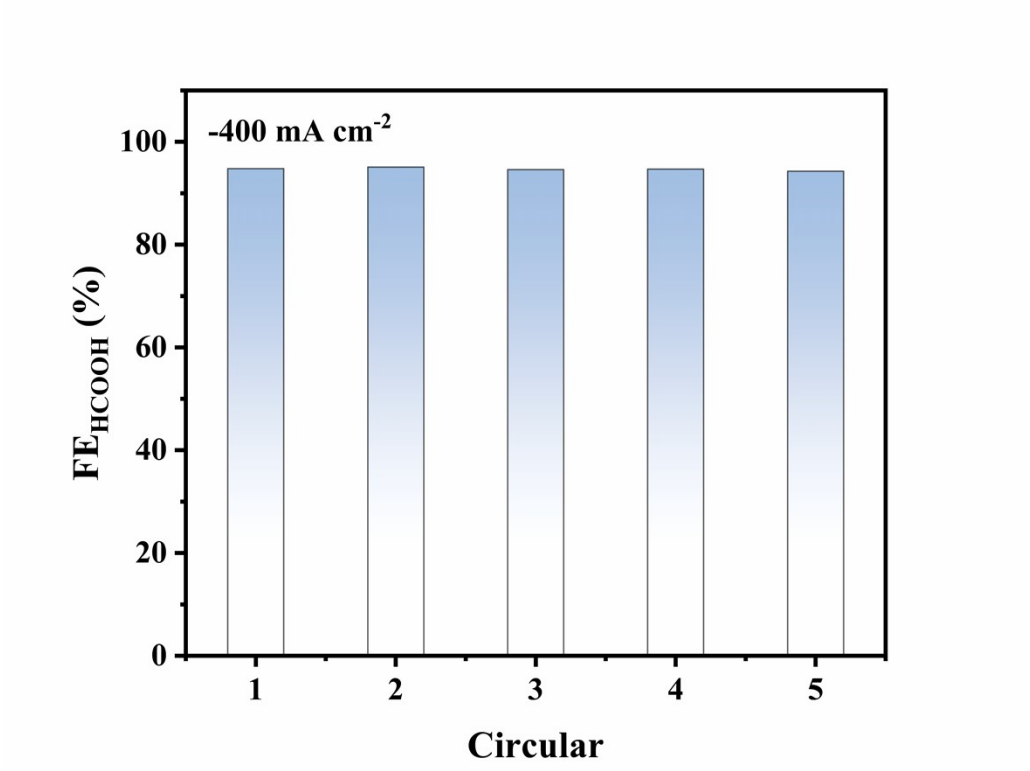

164

165 Fig. S19 The cycle test diagram of OH-Sn@CMK-P.

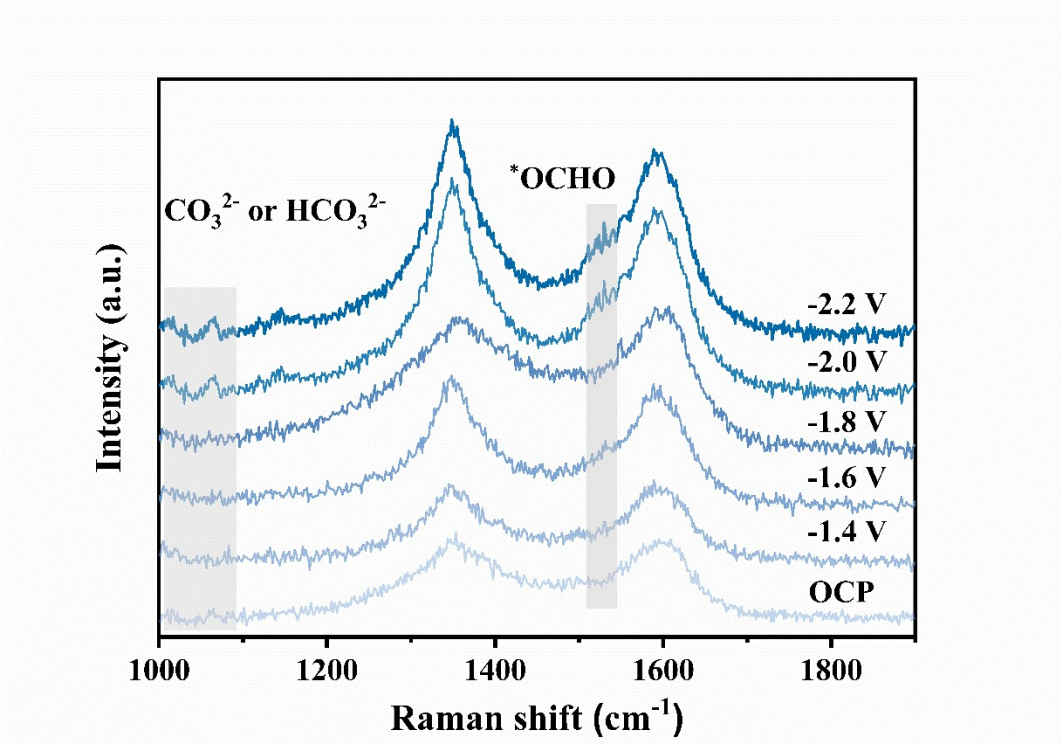

166

167 Fig. S20 In situ Raman spectra recorded at different cathodic potentials over Sn@CMK.

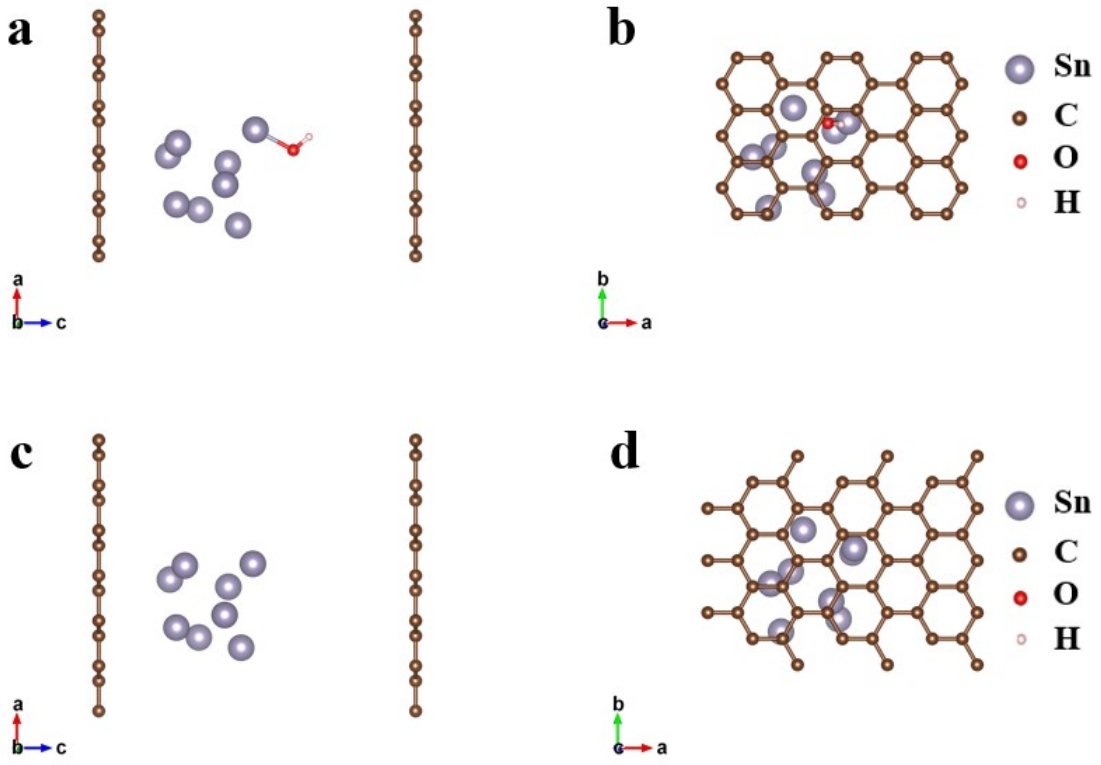

Fig. S21 Schematic catalyst structures: (a) side and (b) top views of OH-Sn@CMK. Schematic catalyst structures: (c) side and (d) top views of Sn@CMK.

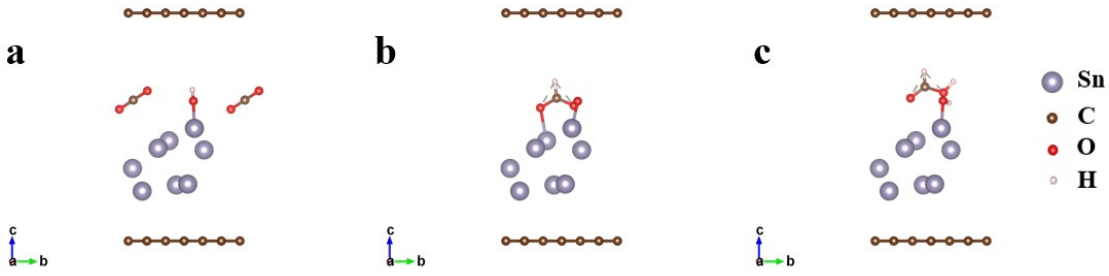

Fig. S22 Intermediate state of HCOOH pathway during CO_2RR over OH-Sn@CMK: (a-c) CO_2*, *OCHO, *HCOOH.

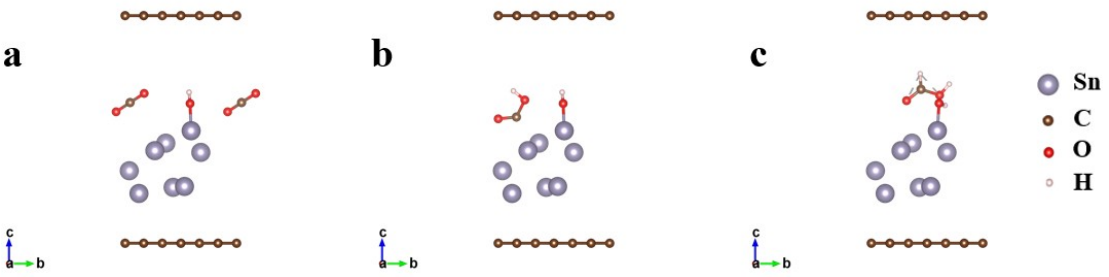

Fig. S23 Intermediate state of HCOOH pathway during CO_2RR over OH-Sn@CMK:

(a-c) CO_2*, *COOH, *HCOOH.

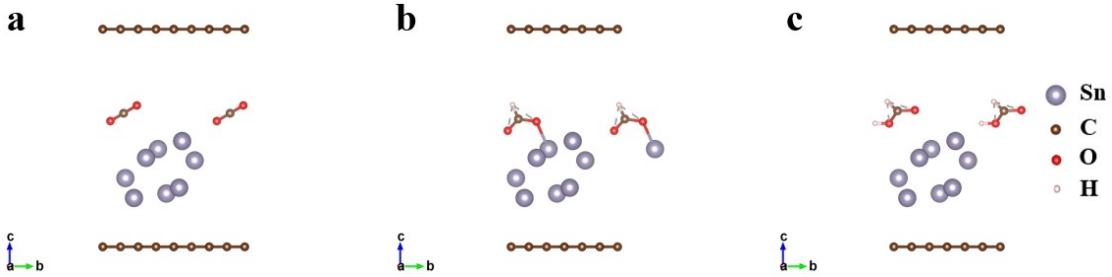

Fig. S24 Intermediate state of HCOOH pathway during CO_2RR over Sn@CMK: (a-c) CO_2*, *OCHO, *HCOOH.

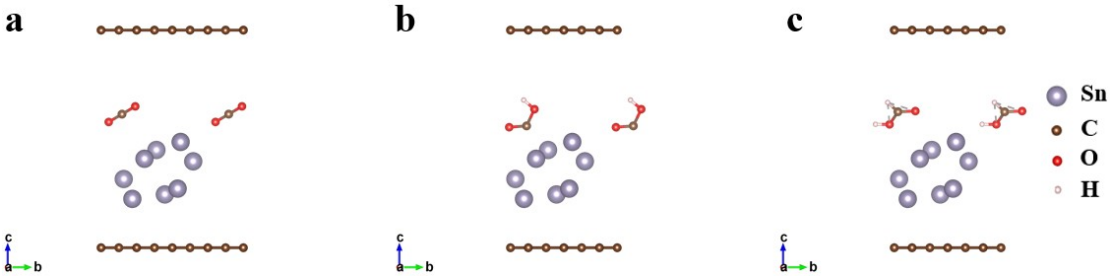

Fig. S25 Intermediate state of HCOOH pathway during CO_2RR over Sn@CMK: (a-c) CO_2*, *COOH, *HCOOH.

REFERENCES

1 G. Kresse, D. Joubert, *Phys. Rev.B.,* 1999, **59**,1758.

2 J. P. Perdew, K. Burke, M. Ermzerhof, *Phys. Rev. Lett*., 1996, **77**, 3865-3868.

3 P. E. Blochl, *Phys. Rev. B*., 1994, **50**, 17953.

4 S. Grimme, J. Antony, S. Ehrlich and H. Krieg, *J. Chem. Phys.*, 2010, **132**, 154104

5 S. Grimme, S. Ehrlich and L. Goerigk, *J. Comput. Chem.*, 2011, **32**, 1456-1465.

6 V. Wang, N. Xu, J.-C. Liu, G. Tang and W.-T. Geng, *Comput. Phys. Commun.*, 2021, **267**, 108033

7 K. Momma, F. Izumi, *J. Appl. Crystallogr*., 2011, **44**, 1272-1276.